SUPPORTING INFORMATION

Flux synthesis, crystal structures, and magnetic ordering of the rare-earth chromium(II) oxyselenides $RE_2CrSe_2O_2$ (RE = La–Nd)

Simon Peschke[1], Valentin Weippert[1], Anatoliy Senyshyn[2], Martin Johann Mühlbauer[2,3,4], Oliver Janka[5], Rainer Pöttgen[5], Stefan Holenstein[6,7], Hubertus Luetkens[6], and Dirk Johrendt[1,]*

[1]Department Chemie, Ludwig-Maximilians-Universität München, D-81377 München, Germany

[2]Heinz Maier-Leibnitz Zentrum (MLZ), Technische Universität München, Lichtenbergstrasse 1, D-85747 Garching, Germany

[3]Helmholtz Institute Ulm for Electrochemical Energy Storage (HIU), Helmholtzstrasse 11, 89081 Ulm, Germany.

[4]Institut for Applied Materials (IAM), Karlsruhe Institute of Technology (KIT), Hermann-von-Helmholtz-Platz 1, 76344 Eggenstein-Leopoldshafen, Germany

[5]Institut für Anorganische und Analytische Chemie, Universität Münster, Corrensstrasse 30, D-48149 Münster, Germany

[6]Laboratory for Muon Spin Spectroscopy, Paul Scherrer Institute, CH-5232 Villigen PSI, Switzerland

[7]Physik-Institut der Universität Zürich, Winterthurerstrasse 190, CH-8057 Zürich, Switzerland

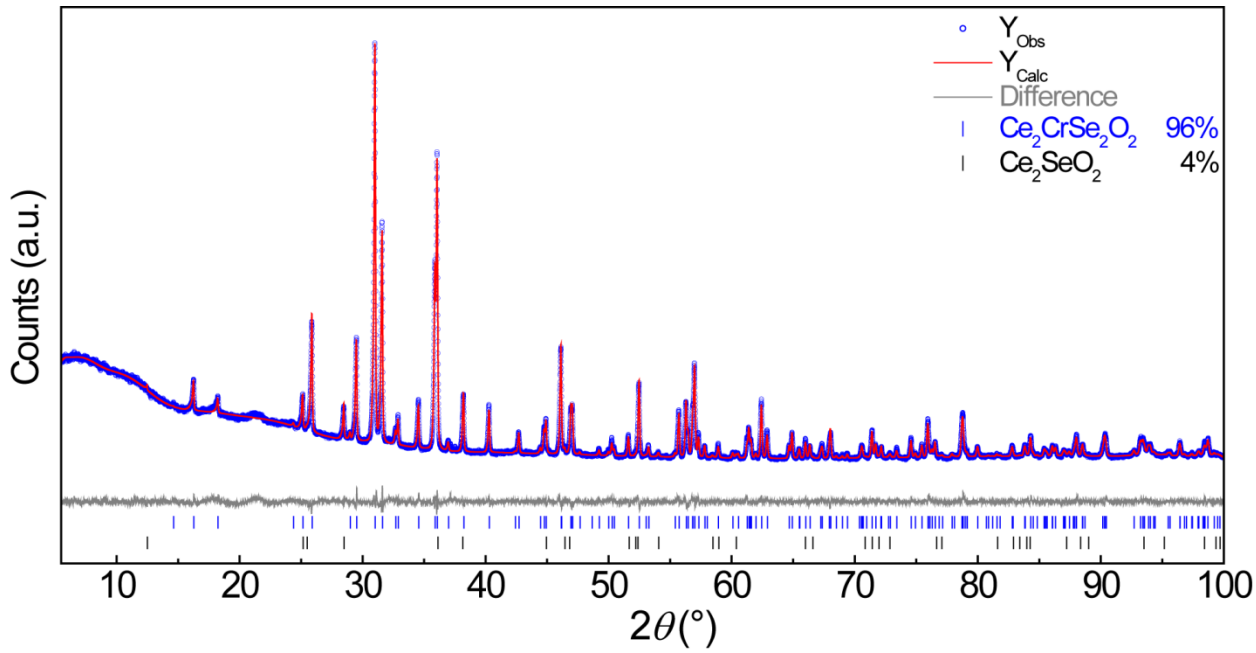

Figure S1. X-ray powder pattern of $Ce_2CrSe_2O_2$ (blue) with Rietveld fit (red) and difference plot (gray) at 300 K.

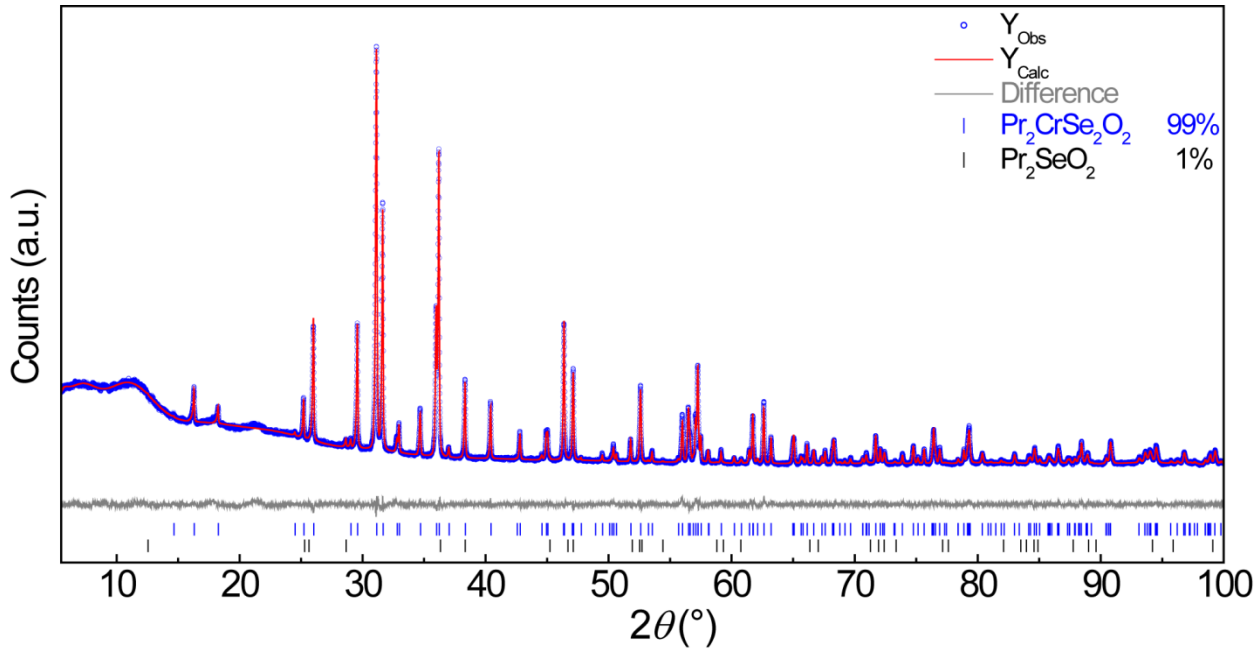

Figure S2. X-ray powder pattern of $Pr_2CrSe_2O_2$ (blue) with Rietveld fit (red) and difference plot (gray) at 300 K.

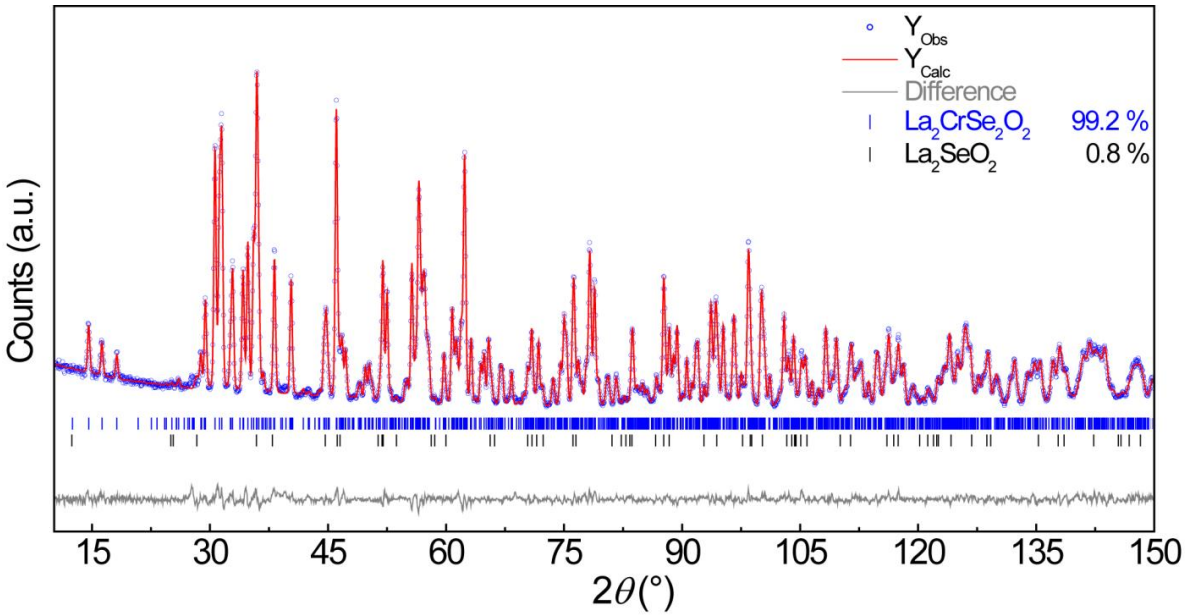

Figure S3. Neutron powder pattern of $La_2CrSe_2O_2$ (blue) with Rietveld fit (red) and difference plot (gray) at 20 K.

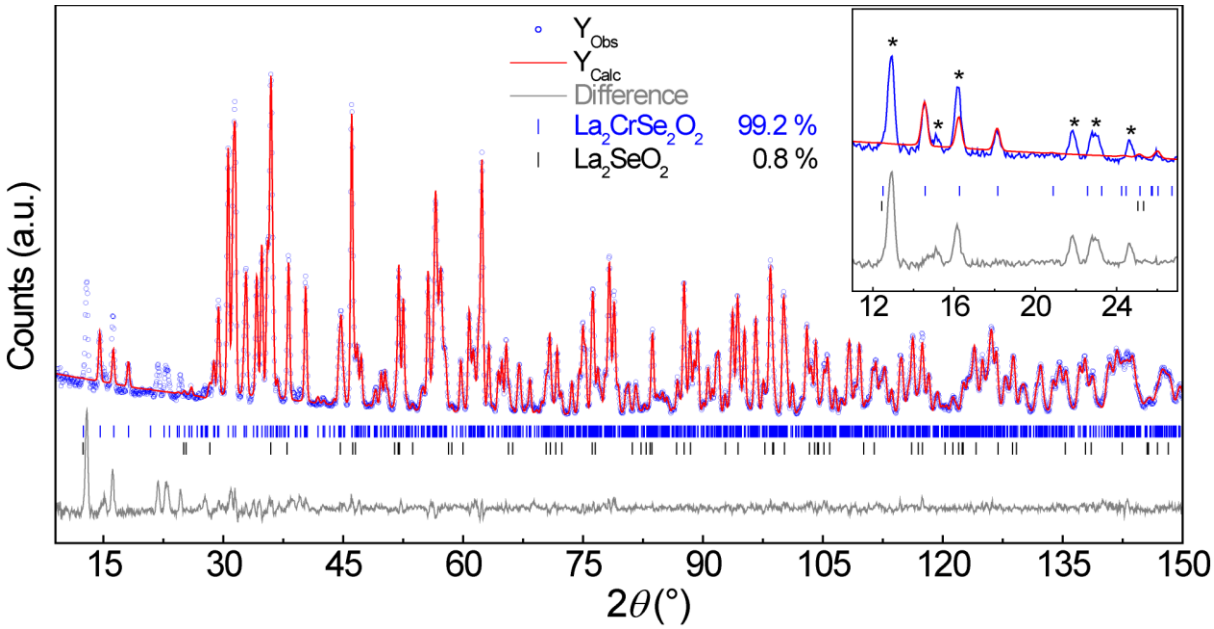

Figure S4. Neutron powder pattern of $La_2CrSe_2O_2$ (blue) with Rietveld fit (red) and difference plot (gray) at 4 K without magnetic model. Inset: Magnification of the pattern. Reflection marked with asterisks are magnetic Bragg reflections.

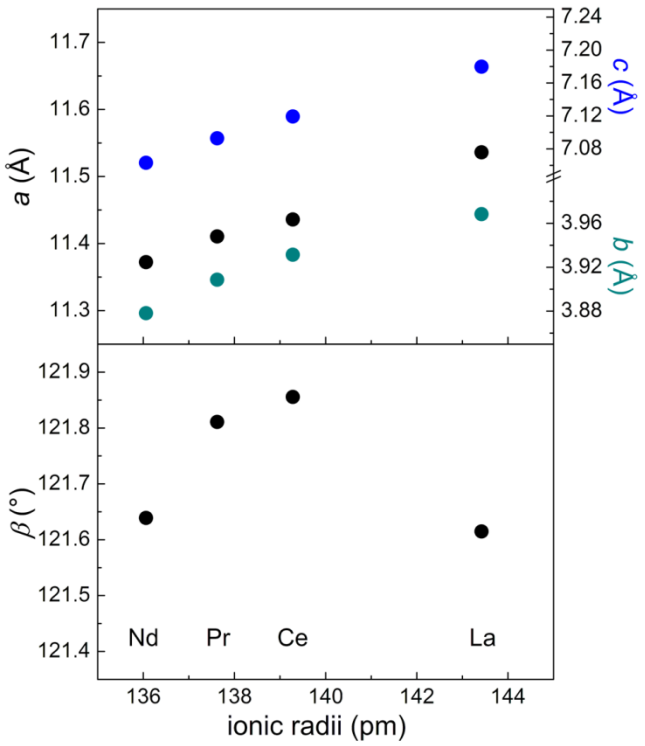

Figure S5. Plot of the lattice parameters *a*, *b* and *c* (top) and the monoclinic angle *β* (bottom) versus the effective ionic radii of the *RE* atom in $RE_2CrSe_2O_2$ (*RE* = La–Nd).

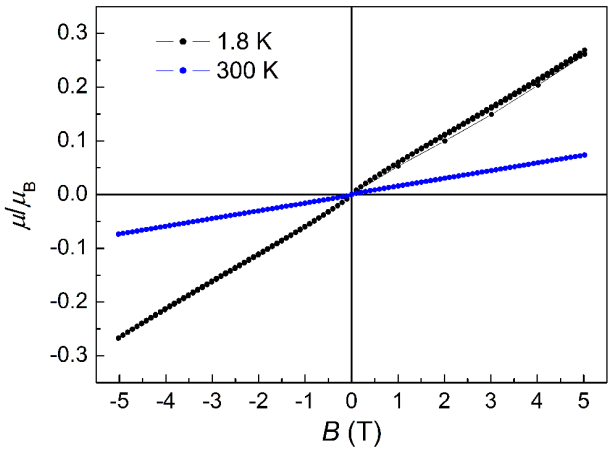

Figure S6. Isothermal magnetizations of $La_2CrSe_2O_2$ at 1.8 (black) and 300 K (blue).

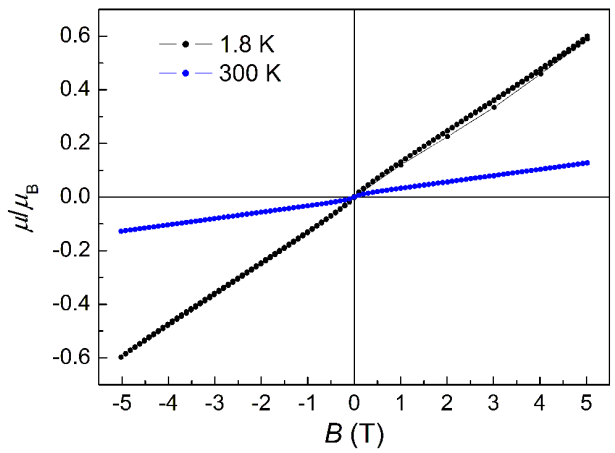

Figure S7. Isothermal magnetizations of $Ce_2CrSe_2O_2$ at 1.8 (black) and 300 K (blue).

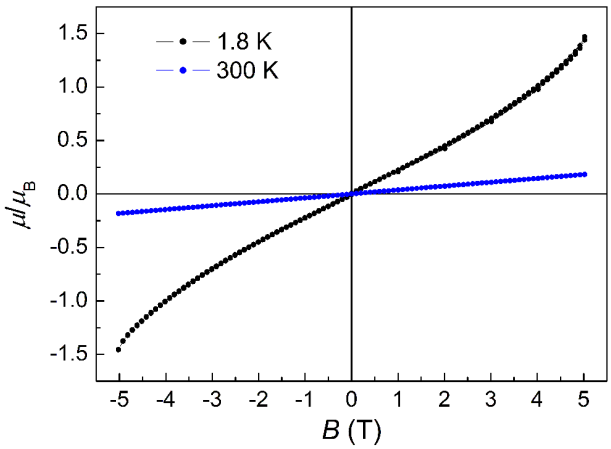

Figure S8. Isothermal magnetizations of $Pr_2CrSe_2O_2$ at 1.8 (black) and 300 K (blue).

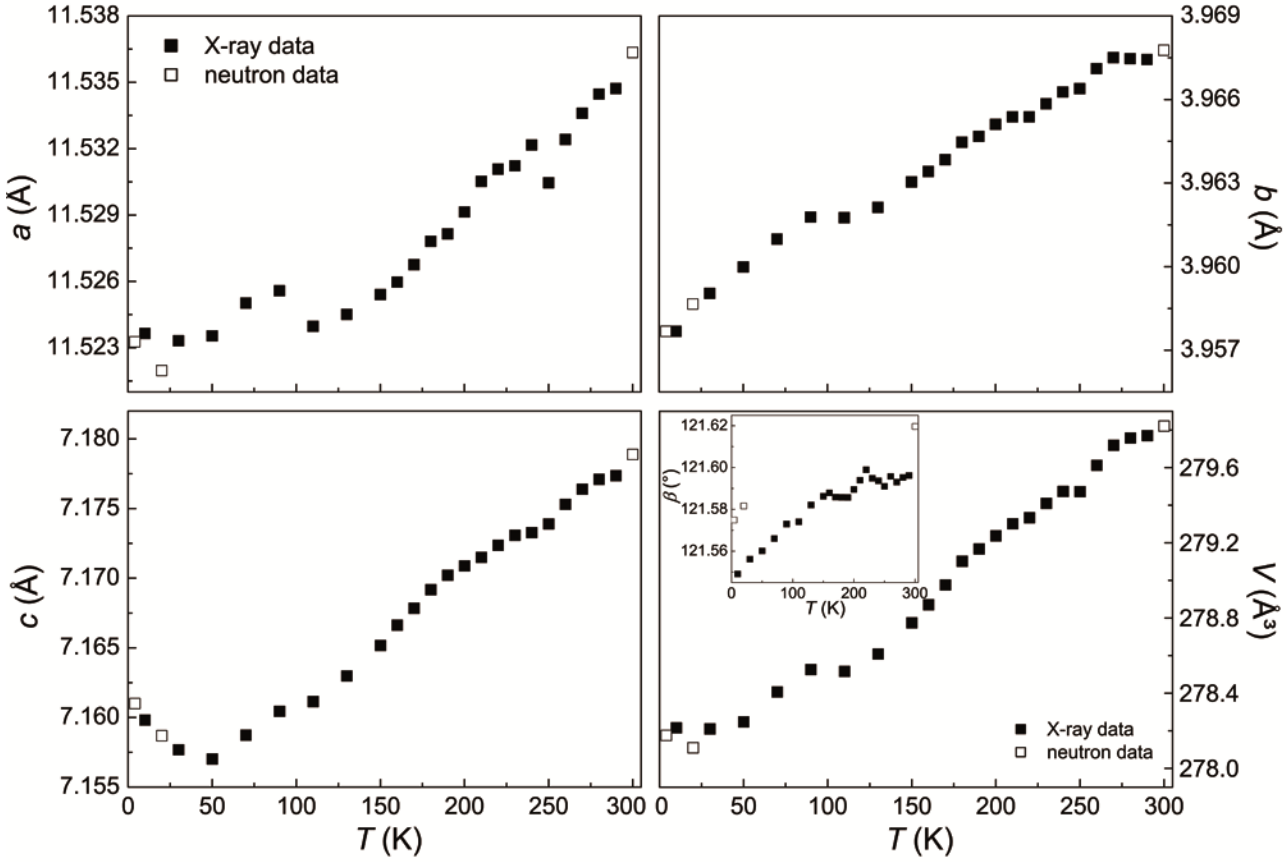

Figure S9. Plots of the lattice parameters *a*, *b*, *c*, *β* (inset) and the cell volume *V* of $La_2CrSe_2O_2$ against the temperature between 4 and 300 K. Filled symbols are data from X-ray powder diffraction, unfilled symbols are from neutron powder diffraction experiments. Error bars are smaller than the data points.

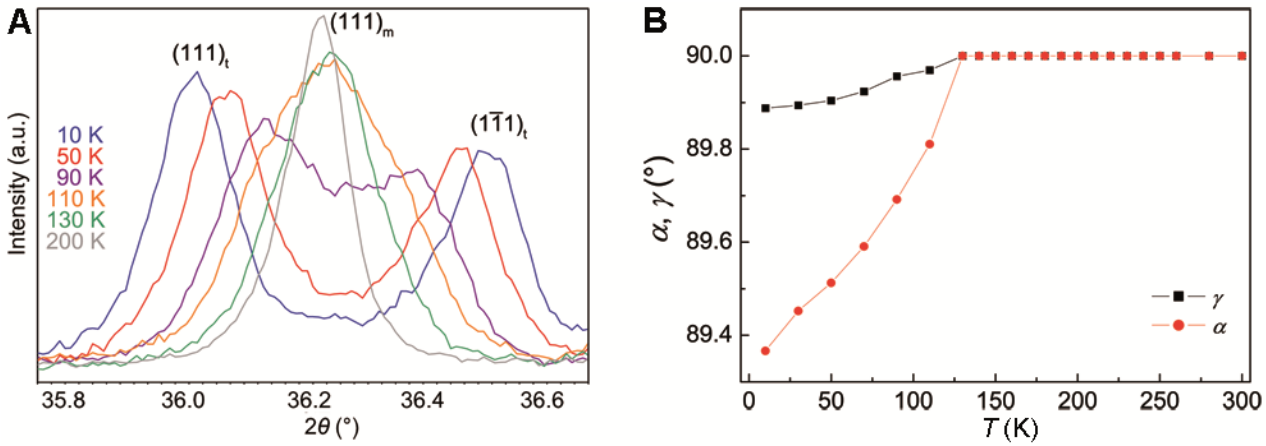

Figure S10. A) Peak splitting of the (111) reflection of the monoclinic phase into (111) and (1$\bar{1}$1) reflections of the triclinic phase at different temperatures in $Ce_2CrSe_2O_2$. B) Evolution of the unit cell angles α and γ of $Ce_2CrSe_2O_2$ upon cooling. Error bars are smaller than the data points.

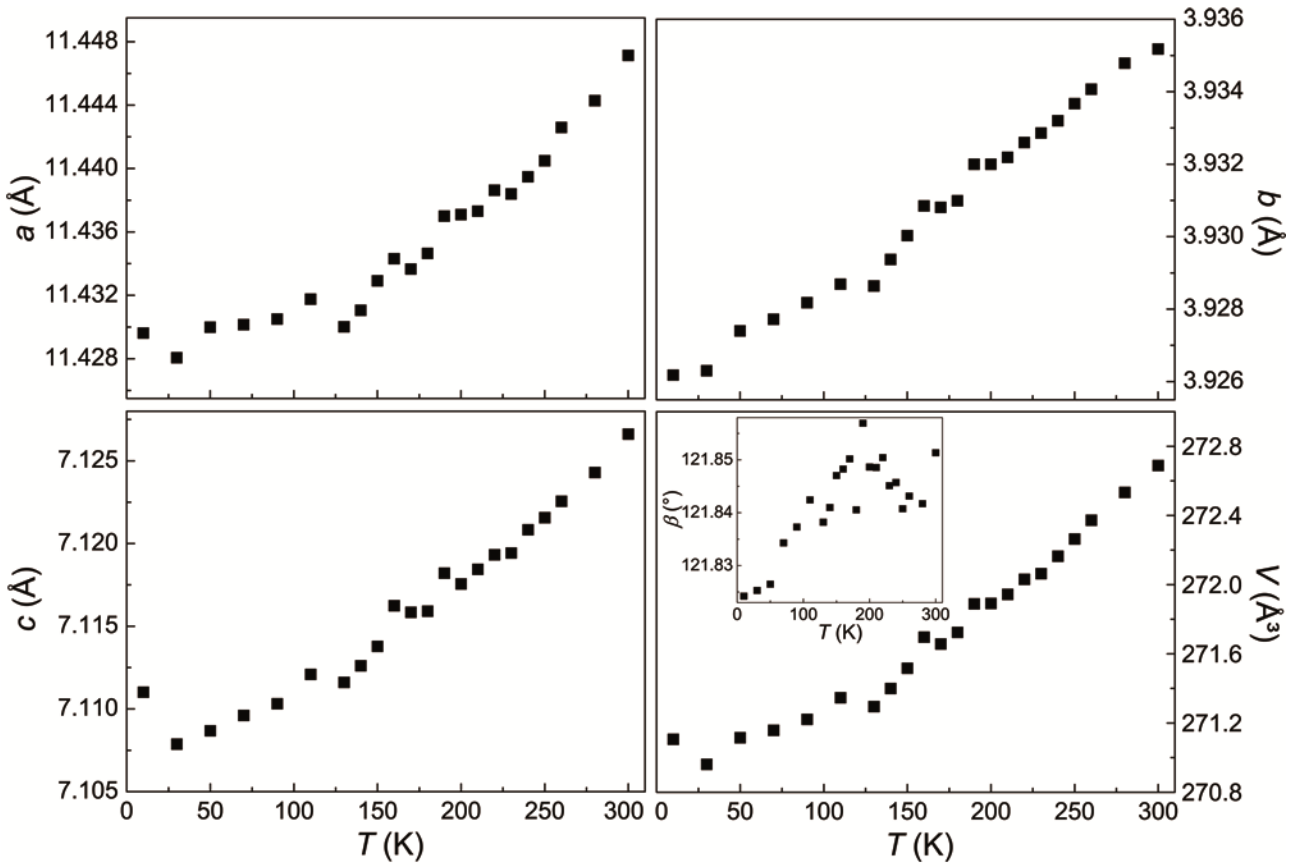

Figure S11. Plots of the lattice parameters *a*, *b*, *c*, *β* (inset) and the cell volume *V* of $Ce_2CrSe_2O_2$ against the temperature between 10 and 300 K. Error bars are smaller than the data points.

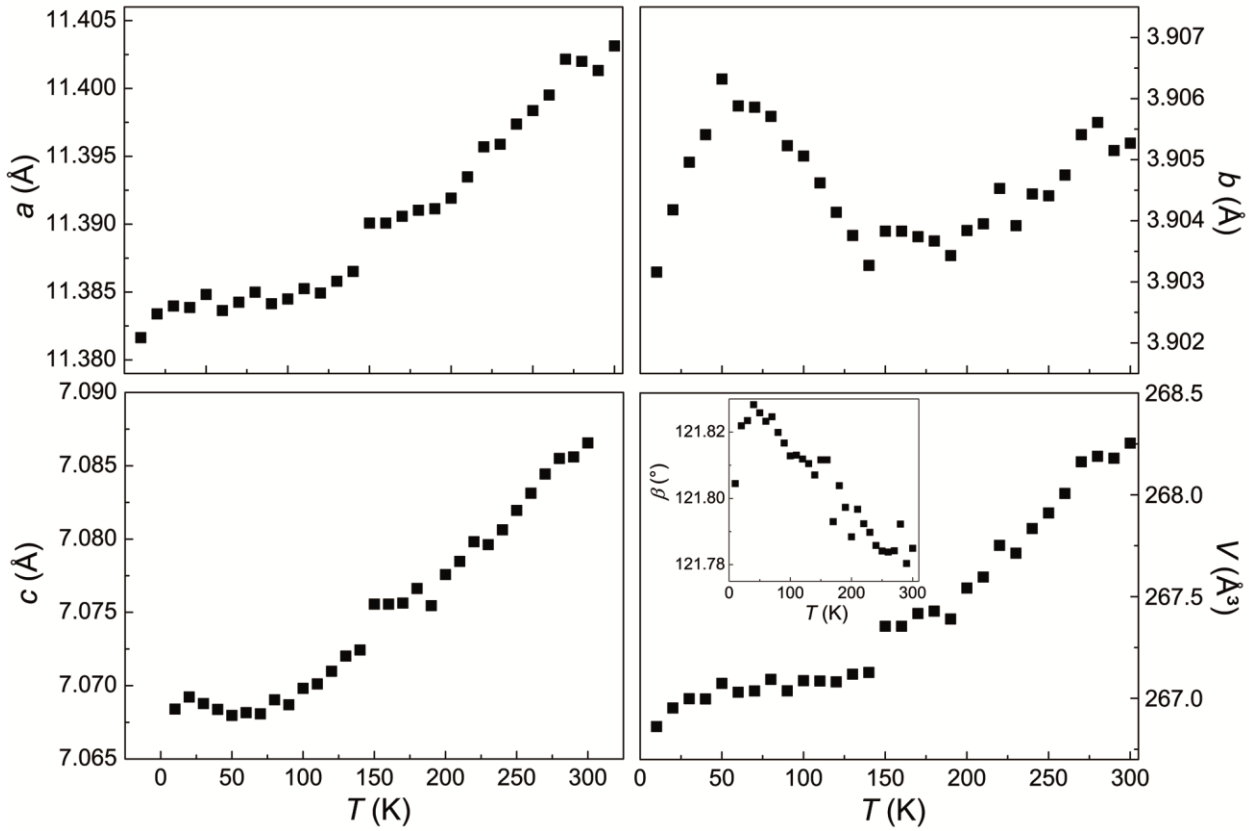

Figure S12. Plots of the lattice parameters *a*, *b*, *c*, *β* (inset) and the cell volume *V* of $Pr_2CrSe_2O_2$ against the temperature between 10 and 300 K. Error bars are smaller than the data points.

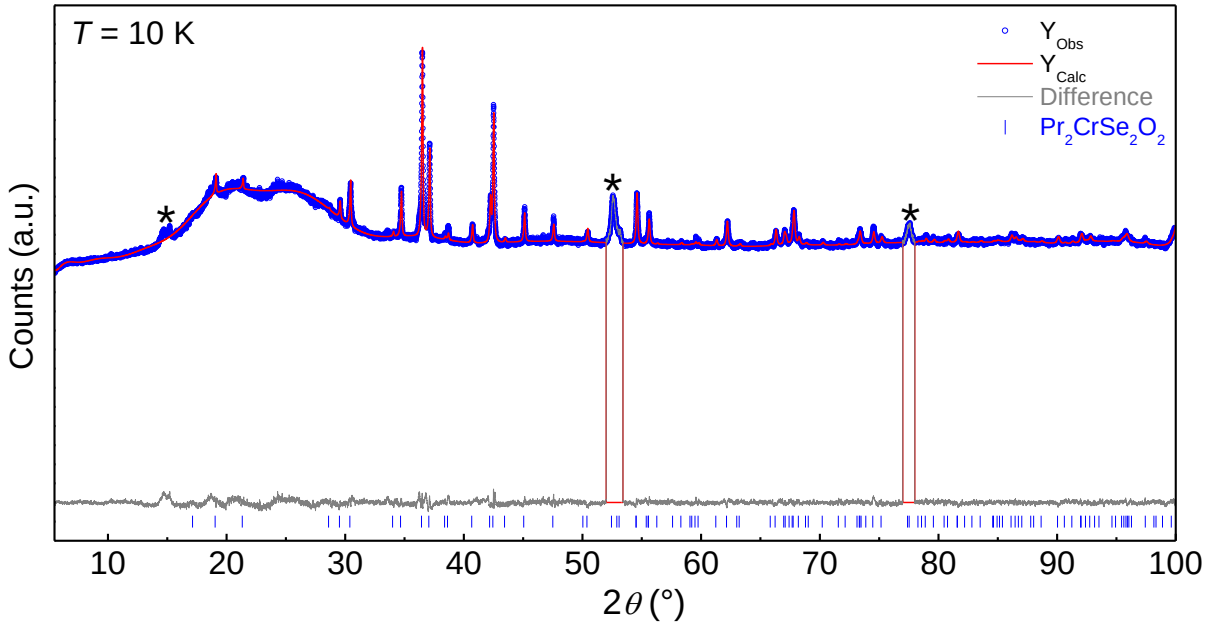

Figure S13. X-ray powder pattern of $Pr_2CrSe_2O_2$ (blue) with Rietveld fit (red) and difference plot (gray) at 10 K. Excluded sections of the diffraction pattern (artefacts from the sample holder and ghost reflections) are marked with asterisks. Refinement in space group *C*2/*m*.

Table S1. Crystallographic data of $La_2CrSe_2O_2$ from single-crystal X-ray diffraction experiments at 300 K.

Formula weight /g mol^{-1}	519.7
Space group	*C*2/*m* (No. 12)
Z	2
Lattice parameters	
a /pm	1153.8(1)
b /pm	396.7(1)
c /pm	717.8(1)
β /°	121.6(1)
V /Å^3, ρ_{xray} / g cm^3	279.7(1), 6.17
Crystal size /mm^3	0.05 × 0.02 × 0.01
Diffractometer	Bruker D8 QUEST
Radiation λ /pm	71.073
Absorption coeff., μ /mm^{-1}	29.8
2Θ range /°	6.66–69.96
Index range (*hkl*)	$h \leq \pm 18$, $k \leq \pm 6$, $l \leq \pm 11$
No. reflections collected	4383
No. unique data, R_{int}, R_σ	679, 0.03, 0.02
No. data with $I > 3\sigma(I)$	607
No. parameters	23
R_1 (obs/all)	0.015/0.019
wR_2 (obs/all)	0.039/0.040
$\Delta\rho$max, $\Delta\rho$min /e Å^{-3}	0.78, −1.05

Atomic parameters and displacement parameters

	Wyckoff	*x*, *y*, *z*	U_{11} (Å²)	U_{22} (Å²)	U_{33} (Å²)
La	4i	0.6932(1), 0, 0.2428(1)	0.0068(1)	0.0055(1)	0.0058(1)
Cr	2d	0, ½, ½	0.0052(4)	0.0112(4)	0.0105(4)
Se	4i	0.9428(1), 0, 0.1840(1)	0.0083(2)	0.0125(2)	0.0091(2)
O	4i	0.8054(3), ½, 0.4197(4)	0.0038(11)	0.0084(11)	0.0075(11)

Selected bond lengths and bond angles

La-O	234.5(1)–241.4(1) pm	Cr-O	200.6(1) pm
La-Se	312.2(1)–334.5(1) pm	Cr-Se	281.9(1) pm
La-O-La	104.8(1)–115.5(1)°	La-O-Cr	107.1(1)–111.9(1)°
Se-Cr-O	89.2(1)–90.8(1)°	Se-Cr-Se	89.5(1)–90.5(1)°

Table S2. Crystallographic data for $La_2CrSe_2O_2$ at 4 and 20 K obtained by neutron powder diffraction experiments.

Temperature /K	4	20
Diffractometer	SPODI	SPODI
Wavelength /nm	1.548	1.548
Space group	$P\bar{1}$	$P\bar{1}$
a, *b*, *c* /pm	1152.3(1), 395.8(1), 716.1(1)	1152.2(1), 395.9(1), 715.9(1)
α, β, γ /°	89.10(1), 121.58(1), 89.87(1)	89.15(1), 121.58(1), 89.87(1)
Cell volume /Å³	278.2(1)	278.1(1)
Data points	3020	2833
Reflections (all phases)	2525	1288
Refined parameters	66	62
R_P, wR_P, χ	0.027, 0.033, 2.90	0.027, 0.034, 3.20

Atomic parameters

	Wyckoff	*x*, *y*, *z*		U_{iso} (pm²)	*x* ,*y*, *z*		U_{iso} (pm²)
La1	2*i*	0.8054(6), 0.2529(7)	-0.0046(11),	38(2)	0.8057(5), 0.2521(6)	-0.0027(10),	38(2)
La2	2*i*	0.6901(6), -0.2642(7)	-0.4924(10),	38(2)*	0.6902(5), -0.2650(6)	-0.4923(10),	38(2)*
Se1	2*i*	0.5589(6), 0.3199(8)	0.0209(15),	38(2)	0.5602(6), 0.3194(8)	0.0219(14),	40(2)
Se2	2*i*	0.0558(6), 0.3132(8)	0.5189(15),	38(2)*	0.0555(6), 0.3141(8)	0.5178(14),	40(2)*
Cr1	1*a*	1, 0, 0		66(6)	1, 0, 0		58(6)
Cr2	1*e*	½, -½, 0		66(6)*	½, -½, 0		58(6)*
O1	2*i*	0.6953(6), 0.0862(9)	-0.4881(13),	56(3)	0.6949(6), 0.0847(10)	-0.4878(14),	66(3)
O2	2*i*	0.8065(6), -0.0752(9)	0.0139(12),	56(3)*	0.8057(6), -0.0769(10)	0.0151(13),	66(3)*

Selected bond lengths and bond angles

	4K	20 K
La1-O1	227.9(1)–235.4(1) pm	228.7(1)–235.2(1) pm
La1-O2	235.4(1) pm	235.5(1) pm
La2-O1	247.9(1) pm	247.6(1) pm
La2-O2	233.5(1)–241.7(1) pm	232.8(1)–241.6(1) pm
La1-Se1	312.1(1) pm	311.0(1) pm
La1-Se2	327.2(1)–339.9(1) pm	327.1(1)–338.3(1) pm
La2-Se1	321.6(1)–340.9(1) pm	321.0(1)–342.7(1) pm
La2-Se2	312.8(1) pm	313.0(1) pm
Cr1-O2	200.2(1) pm	200.7(1) pm
Cr2-O1	199.9(1) pm	199.7(1) pm
Cr1-Se2	272.4(1)–288.1(1) pm	273.3(1)–288.2(1) pm
Cr2-Se1	274.5(1)–291.3(1) pm	273.8(1)–290.9(1) pm

La-O-La	102.4(1)–117.3(1)°	102.4(1)–117.1(1)°
La-O-Cr	105.1(1)–114.6(1)°	105.4(1)–114.6(1)°
Se-Cr-O	87.6(1)–92.4(1)°	87.5(1)–92.5(1)°
Se-Cr-Se	88.7(1)–91.3(1)°	89.0(1)–91.0(1)°

*Note: Following constraints were used: U_{iso}(La2) = U_{iso}(La1), U_{iso}(Se2) = U_{iso}(Se1), U_{iso}(Cr2) = U_{iso}(Cr1), U_{iso}(O2) = U_{iso}(O1).

Muon spin rotation and relaxation

The quantitative analysis of the ZF-μSR data reveals that besides the two oscillating components two further non-oscillating contributions have to be taken into account to fully describe the low temperature spectra. Therefore the following polarization function has been used for the analysis of the ZF-μSR data.

$$\boldsymbol{P(t) = \frac{2}{3}\sum_{i=1}^{4} a_i e^{-\lambda_i t} cos(2\pi f_i t) + \frac{1}{3} e^{-\lambda_L t}}$$

The sum of a 2/3 and a 1/3 fraction of the signal originates from the powder average of the internal fields with respect to the initial muon spin direction in our polycrystalline sample. The 2/3 transverse signal represents the muon spin components that are perpendicular to the internal fields while the 1/3 signal fraction stems from the muon spin components which are parallel to the internal fields. The a_i are the amplitudes of the different signals which were determined at low temperatures and then kept fix for the higher temperature data (a_1 = 0.19, a_2 = 0.06, a_3 = 0.38, a_4 = 0.37, f_3 = f_4 = 0). The transverse relaxation rates λ_i are a measure for the width of the probed field distribution while the longitudinal or spin-lattice relaxation rate λ_L is solely related to the dynamics of the magnetic system under investigation.

Table S3. List of the starting atomic ratios of rare-earth oxides, rare-earth metals, chromium and selenium.

	M **(g/mol)**	***n*** **(mmol)**	***m*** **(mg)**
La_2O_3	325.8091	0.2566	83.6
La	138.9055	0.2566	35.6
Cr	51.9961	0.3848	20.0
Se	78.96	0.7696	60.8
CeO_2	172.1148	0.3830	65.9
Ce	140.116	0.3830	53.7
Cr	51.9961	0.3830	19.9
Se	78.96	0.7661	60.5
Pr_2O_3	329.814	0.2546	84.0
Pr	140.908	0.2546	35.9
Cr	51.9961	0.3819	19.9
Se	78.96	0.7638	60.3
Nd_2O_3	336.482	0.2514	84.6
Nd	144.242	0.2514	36.3
Cr	51.9961	0.3771	19.6
Se	78.96	0.7542	59.6